Article

Influence of Local Thermodynamic Non-Equilibrium to Photothermally Induced Acoustic Response of Complex Systems

Slobodanka Galovic [1,*], Aleksa I. Djordjevic [2], Bojan Z. Kovacevic [2,3], Katarina Lj. Djordjevic [1] and Dalibor Chevizovich [1,*]

1. Vinca Institute of Nuclear Sciences, National Institute of the Republic of Serbia, University of Belgrade, Mike Petrovica Alasa 12-14, 11001 Belgrade, Serbia; katarina.djordjevic@vin.bg.ac.rs
2. Faculty of Physics, University of Belgrade, Studentski trg 12, 11001 Belgrade, Serbia; djordjevicaleksa98@gmail.com (A.I.D.); bojan.kovacevic@pmf.unibl.org (B.Z.K.)
3. Faculty of Natural Sciences and Mathematics, University of Banja Luka, Mladena Stojanovica 2, 78000 Banja Luka, Republic of Srpska, Bosnia and Herzegovina
* Correspondence: bobagal@vin.bg.ac.rs (S.G.); cevizd@vin.bg.ac.rs (D.C.)

Abstract: In this paper, the time-resolved model of the photoacoustic signal for samples with a complex inner structure is derived including local non-equilibrium of structural elements with multiple degrees of freedom, i.e., structural entropy of the system. The local non-equilibrium is taken into account through the fractional operator. By analyzing the model for two types of time-dependent excitation, a very short pulse and a very long pulse, it is shown that the rates of non-equilibrium relaxations in complex samples can be measured by applying the derived model and time-domain measurements. Limitations of the model and further directions of its development are discussed.

Keywords: heat transfer; irreversibility; local non-equilibrium; time delayed equation; fractional calculus; subdiffusion; Mittag-Leffler function; time-domain photoacoustic

1. Introduction

Photoacoustic (PA) and other photothermal (PT) techniques are non-destructive experimental methods based on the recording of detectable phenomena produced by optically induced heat transfer across the illuminated sample [1–8]. These techniques have been developed for the last half century and are increasingly being applied to measure the thermal properties of various samples [9–16].

In PA measurement, the pressure fluctuations in the gaseous surroundings of the optically heated sample are recorded [1–3]. They are proportional to the surface temperature variations of the optically excited sample [1,17]. To relate these fluctuations to sample properties, it is necessary to develop a theoretical description of heat transfer across the illuminated sample and to calculate surface temperature variations based on this description.

Classical heat conduction theory [18] was established more than 150 years ago and is still found in textbooks and most of the engineering and scientific literature is related to the problem of heat transport because it is consistent with the basic laws of thermodynamics. However, classical thermodynamics contains some assumptions that limit its domain of validity [19–22]. One of these assumptions is the local equilibrium assumption for non-equilibrium situations such as heat transport. Namely, classical thermodynamics considers that all sub-systems of a thermodynamic system are in local equilibrium while the system is not in equilibrium [19]. This assumption is valuable only if all subsystems relax at rates much larger than the rate of system enthalpy changes [23,24]. Otherwise, the influence of local relaxations must be taken into account [25–36].

The rates of subsystem relaxations in crystal solids are large [37]. Therefore, one does not expect their influence on heat transfer in the usual measurement ranges of standard

experiments based on heat transfer, such as PAs and other PT techniques. The theoretical estimations of the relaxation rates in complex systems are much less reliable due to the large structural entropy of these systems; however, they are expected to be much slower than in crystals [29,37]. Besides, many calorimetric experiments show that the heat transport within complex systems such as glasses, liquid crystals, polymers, biopolymers, biological tissues, etc. deviates from the corresponding standard Fourier's theory of heat conduction [30–37], indicating a possible influence of non-equilibrium relaxations in the usual measurement range of PT techniques [38].

In this paper, we derive a generalized model of a photothermally induced acoustic signal, including local relaxation in the sample with a complex inner structure. Our objective is to investigate whether PA measurements could be employed in the estimation of non-equilibrium relaxation rates in complex systems.

The structure of the paper is as follows: After this introductory chapter, in Section 2, we briefly presented the fractional theory of heat conduction, which includes kinetic relaxations due to local non-equilibrium. We showed that kinetic relaxations can be connected with a microscopic approach based on fractional statistical physics and the kinetic memory of substantial media. Using the proposed fractional theory in Section 3, a model of the spectral function of the PA signal was derived by applying the Laplace transform. After that, by applying the inverse Laplace transform to the spectral function of the PA signal for a thin sample, a model of the time-dependent PA signal generated by optical pulse excitation was derived. In Section 4, the time-dependent PA signal was analyzed for samples with a complex internal structure of different thicknesses. It has been shown that kinetic relaxations affect the slope and magnitude of the time-resolved PA signal, indicating that this measurement technique can be employed in the observation of local non-equilibrium in complex systems.

2. Theory of Heat Conduction including the Non-Equilibrium Relaxation

The classical theory of heat conduction is based on the law of conservation of energy (First Law of Thermodynamics, Equation (1)) and Fourier's constitutive relation, Equation (2), which satisfies the Second Law of Thermodynamics [18,39]:

$$c_p \frac{\partial T(x,t)}{\partial t} + div \overrightarrow{q}(x,t) = 0 \tag{1}$$

$$\overrightarrow{q}(x,t) = -k \frac{\partial T(x,t)}{\partial x} \tag{2}$$

In the above equations, $T(x,t)$ denotes the change in the equilibrium temperature, and $\overrightarrow{q}(x,t)$ denotes the heat flux.

The first term of Equation (1) denotes the rate of change of internal energy $\partial e(x,t)/\partial t$ [27], while the second term, the divergence of the heat flux caused by the appearance of a temperature gradient inside the sample, refers to the dissipation of energy inside the sample and is related to the increase in entropy of the system during the process of energy exchange between the system and its environment [23,40]. The volume heat capacitance of a system $c_p = \rho C_p$ tells us how much heat per unit volume the system will absorb from its surroundings if we change its temperature by a small amount. Symbols C_p and ρ signify mass heat capacitance and mass density, respectively, and symbol k signifies thermal conductivity.

Substituting Equation (2) into Equation (1) gives the classic heat conduction equation [18]:

$$\frac{\partial^2 T(x,t)}{\partial x^2} - \frac{1}{D} \frac{\partial T(x,t)}{\partial t} = 0 \tag{3}$$

where D denotes thermal diffusivity of the system and it is defined as the ratio of thermal conductivity k and volume heat capacitance c_p, $D = k/c_p$.

Equation (3) has been used for more than a century to describe heat transport processes in the condensed phase and to explain and process dynamic calorimetric experiments [18]. However, numerous experiments performed in the last fifty years on systems with a complex internal structure cannot be explained by the application of classical theory. A number of such experiments are explained by the introduction of complex heat capacitance [23,25,26,38], indicating that there is an approximation in the First Law of Thermodynamics given by Equation (1) that limits the domain of applicability of the classical theory [23,38].

From a thermodynamic point of view, the First Law of Thermodynamics given in the form of Equation (1) assumes that the exchange of energy between a system and its environment is a reversible process when the dissipation due to the appearance of a temperature gradient is neglected (e.g., in the case of small-sized samples) [40]. This further means that the increase in entropy due to the thermodynamic process of energy exchange is ignored [23] in this case; that is, this law assumes the local equilibrium of all subsystems even though the whole system is not in thermodynamic equilibrium with the environment [19–22]. This approximation can be removed by introducing one more state variable (in addition to pressure and temperature), which is called affinity [23,41,42].

Generally, at constant temperature and pressure, affinity can be regarded as the advancement of an internal parameter (internal degree of freedom) of the system or as thermodynamic potential for the system undergoing a physic-chemical transformation, i.e., as a generalized driving force that vanishes when the system is at equilibrium. Prigogine, De Groot, and Mazur [41] defined an internal space of configuration of the system, where each degree of freedom is represented by a continuing variable representing a coordinate of the internal space. By analogy with heat diffusion in classical theory, where heat is lost along the spatial direction defined by hot and cold points, in this representation, heat is lost by diffusion along the coordinate defined by the degree of freedom inside the internal space of configuration, which participates in the entropy productions [23]. It could be related to the kinetic memory of the system, which comes into expression when the time scale of observing the process (of the experiment) is approximately equal to or less than the relaxation time of kinetic relaxations [19–23]. Unfortunately, reliable estimates of kinetic relaxation times do not exist, and the existing ones range in ten orders of magnitude [37]. It is difficult to say on what scale the influence of local non-equilibrium should be expected to appear in various substantial media. But some experimental results related to heat flow across biological tissues and polymeric materials indicate that deviations from the prediction of classical heat conduction theory can be observed on the time scale of existing photothermal experiments [38]. Since the classical theory is widely spread in textbooks and the scientific literature outside the narrow circle of researchers dealing with dissipative processes, these effects are most often ignored, or if shown, they are attributed to some other influences.

When a complex system with an internal degree of freedom absorbs energy from (or releases it to) its environment, it is in a non-equilibrium state, but if this state is close to equilibrium, the internal energy can be described through convolutional integral as it is described in linear response theory [27,28].

$$e(x,t) - e_0 = c_p \left[\Phi(0)T(x,t) + \int_0^t \frac{d\Phi(t')}{dt'} T(x,t-t')dt' \right] \tag{4}$$

where c_p is the equilibrium volume heat capacitance and $\Phi(t)$ is kinetic memory kernel that must satisfies relations $\Phi(t=0) = 1$ and $\Phi(t \to \infty) = 0$ [25].

In essence, the above integral relation introduces a phase lag between change of internal energy and change of local equilibrium temperature, $e(x, t + \tau) \sim T(x, t)$, meaning that under the local non-equilibrium condition the kinetic temperature (i.e., internal energy e) relaxes to the local equilibrium temperature T after time τ [21,22].

The assumption about exponentially fading memory kernel $\Phi(t)$ leads to the generalized theory of heat conduction with complex heat capacitance that is widely used in the analysis of the calorimetric measurement of a complex system. However, microscopic approach to derivation of heat conduction equation in complex media that consider experimentally observed anomalous diffusive effects suggests the following fractional relation between temperature rate and internal energy rate [43–50]:

$$\frac{\partial e(x,t)}{\partial t} = c_{pv}\frac{\partial^v T(x,t)}{\partial t^v} \tag{5}$$

where the Riemann–Liouville definition of fractional derivative is used, for an arbitrary function $f(x,t)$ [49–53]:

$$\frac{\partial^v f(x,t)}{\partial t^v} = \frac{1}{\Gamma(1-v)}\frac{\partial}{\partial t}\int_0^t \frac{f(x,t')}{(t-t')^v}dt',\ 0 < v < 1 \tag{6}$$

and $\Gamma(v)$ is Gamma function defined via convergent improper integral: $\Gamma(v) = \int_0^\infty t^{v-1}e^{-t}dt$, $0 < v$. With c_{pv} is denoted fractional volume heat capacitance $c_{pv} = c_p\tau^{v-1}$ and τ is kinetic relaxation time. In this microscopic theory, the fractional exponent v and fractional volume heat capacitance c_{pv} are associated with anomalous diffusion effects, that is, with the experimentally observed deviation of the mean square length of heat carriers from the linear time dependence [43,49].

Substituting Equation (6) into Equation (5) and comparing with Equation (4), assuming zero initial conditions, it can be concluded that anomalous diffusion effects can be associated with local non-equilibrium and power law fading memory kernels. Consequently, the non-equilibrium process is governed by the kinetic relaxation time through the fractional heat capacitance c_{pv} and fractional exponent v. In the absence of anomalous diffusion effects ($v = 1$), fractional heat capacitance is reduced to the equilibrium heat capacitance, and fractional derivatives given by Equation (6) are reduced to integer derivatives, meaning that the change in internal energy does not show a delay in relation to the change in equilibrium temperature.

A fractional-order differential calculus is a generalization of the integer-order integral and derivative to real or even complex order [50–52]. This idea first emerged at the end of the seventeenth century and has been developed in the area of mathematics throughout the eighteenth and nineteenth centuries. More recently, by the end of the twentieth century, it turned out that some physical phenomena can be modeled more accurately when fractional calculus is used [53–59].

By substituting Equation (5) into Equation (1) and by substituting Equation (2) into Equation (1), a generalized description of heat conduction through complex systems is obtained, which includes local non-equilibrium through the fractional exponent v and fractional heat capacity c_{pv}:

$$c_{pv}\frac{\partial^v \vartheta(x,t)}{\partial t^v} - k\frac{\partial^2 \vartheta(x,t)}{\partial x^2} = 0 \tag{7}$$

while the constitutive relation that satisfies the Second Law of Thermodynamics remains the same Equation (2).

In the Equation (7), $\vartheta(x,t) = T(x,t) - T_0$ is the temperature variation of the system with respect to the temperature at which the sample was in thermodynamic equilibrium with the environment, and T_0 signifies temperature of ambient.

It is important to note that the same generalized equation of heat conduction, Equation (7), was derived from the point of view of statistical physics by using various approaches [43–45].

3. Model of PA Signal including Local Thermal Non-Equilibrium in the Sample

Photothermally induced acoustic responses involve multiple coupled physical phenomena (e.g., laser-matter interaction, heat conduction, acoustic wave propagation), which exhibit dynamics at multiple scales [1–8]. Additionally, these phenomena are governed by various physical properties of the sample (optical, thermal, elastic, electronic, etc.), leading to very complex multiparametric models of PA signals [9]. This not only significantly complicates the solution of the inverse PA problem but can also make its solution non-unique and less accurate [60], preventing the application of PA methods in measuring the thermal properties of the sample. Therefore, when solving the direct PA problem, one often resorts to the development of approximate models, which take into account only those processes that are dominant in the real measurement range.

In this section, we developed a direct model of the PA signal recorded in a gas-microphone configuration of the experiment, based on the widespread Rosencwaig–Gersho (RG) [1] theory of the formation of pressure fluctuations in a closed cell of small volume (in which the length of the gas column is smaller than the wavelength of the acoustic waves). In addition, we considered that the sample can be considered thermally homogeneous, but that due to its complex internal structure, kinetic relaxations, i.e., the influence of local thermal non-equilibrium, should be taken into account.

We observe an optically opaque sample that is illuminated uniformly over the entire surface, Figure 1.
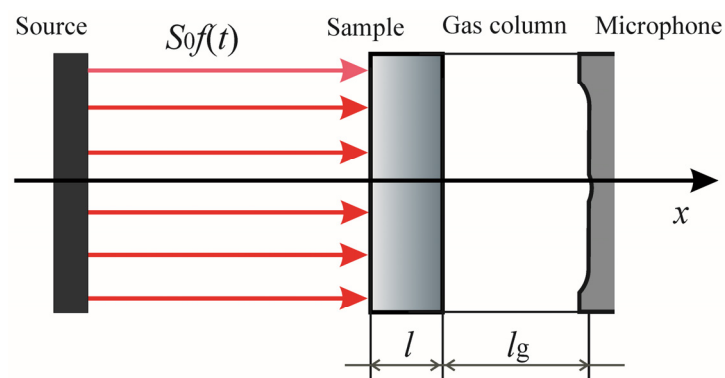
Figure 1. Geometry of the problem.

The sample is surrounded by air, and air conducts heat much more poorly than the sample [61]. In difference to frequency PA methods where harmonic excitation of various frequencies is used, we consider that the time dependence of the optical excitation can be described by unity pulse for very short optical pulse:

$$f(t) = \delta(t) = \begin{cases} 1 & t = 0 \\ 0 & t \neq 0 \end{cases} \tag{8}$$

and by Heaviside function for very long optical pulse:

$$f(t) = h(t) = \begin{cases} 1 & t \geq 0 \\ 0 & t < 0 \end{cases} \tag{9}$$

where the system was in thermodynamic equilibrium with the environment at ambient temperature T_0 for $t < 0$. That time dependence of optical excitation can describe time-domain PA experiments very well [62].

When the sample is illuminated, the part of the excitation EM energy is absorbed, and part of the absorbed energy is converted into heat on the surface of the sample (due to the fact that the sample is optically opaque). In other words, the excitation optical beam leads to the formation of an excitation heat flux on the illuminated surface of the

sample, which follows the dynamics of the optical excitation due to very fast (infinitely fast) de-excitation–relaxation processes [63]:

$$S(x,t) = (1-R)\eta I_0 \delta(x) f(t) = S_0 \delta(x) f(t) \tag{10}$$

where $S_0 = (1-R)\eta I_0$ is absorbed electromagnetic flux, R is coefficient of optical reflection, η is quantum coefficient of conversion of electromagnetic energy into heat, and I_0 is excitation electromagnetic flux.

Symbol $\delta(x)$ in Equation (10) signifies Dirac δ function:

$$\int_{-\infty}^{+\infty} \delta(x) dx = \begin{cases} 1 & x = 0 \\ 0 & x \neq 0 \end{cases} \tag{11}$$

Inside the sample, a perturbation of the thermodynamic state occurs, and heat flow and heat flux appear, which tend to bring the system into a new thermodynamic equilibrium with the environment. Based on the theoretical model presented in the previous section, the propagation of optically generated heat through the sample can be described by the following system of partial differential equations:

$$\frac{\partial^2 \vartheta(x,t)}{\partial x^2} - \frac{1}{D_v} \frac{\partial^v \vartheta(x,t)}{\partial t^v} = -\frac{1}{k} S_0 f(t) \delta(x) \tag{12}$$

$$q(x,t) = -k \frac{\partial \vartheta(x,t)}{\partial x} \tag{13}$$

where $D_v = k/C_{pv}$ is fractional heat diffusivity.

We suppose zero initial conditions and zero flux boundary conditions (because the air is a much better heat conductor [61]). Substituting Equation (10) in Equation (12) and by integrating this equation about point $x = 0$ (and by using Equation (11)), the problem is reduced to system of homogeneous partial differential equations:

$$\frac{\partial^2 \vartheta(x,t)}{\partial x^2} - \frac{1}{D_v} \frac{\partial^v \vartheta(x,t)}{\partial t^v} = 0 \tag{14}$$

$$q(x,t) = -k \frac{\partial \vartheta(x,t)}{\partial x} \tag{15}$$

with inhomogeneous boundary condition in point $x = 0$:

$$q(x = 0, t) = S_0 f(t) \tag{16}$$

$$q(x = l, t) = 0 \tag{17}$$

The heat transfer is described in the 1D spatial dimension due to the fact that the heat source appears as a surface source in a uniformly illuminated sample [64].

Based on Equations (14)–(17), it can be seen that the entire problem is described by fractional linear partial differential equations. Such equations, as well as integer linear partial differential equations, can be solved using different methods, e.g., master equation approach [65]. In this paper, we use the Laplace transform because this integral transformation method enables simultaneous analyzes of spectral function (significant for frequency PA methods) and time-resolved PA signals (significant for time-domain photoacoustics).

By applying the Laplace transform to Equations (14)–(17), the above system of equations is reduced to a system of linear differential equations with complex coefficients:

$$\frac{d^2 \overline{\vartheta}(x,s)}{dx^2} - \overline{\sigma}^2 \overline{\vartheta}(x,s) = 0 \tag{18}$$

$$\overline{q}(x,s) = -\frac{1}{\overline{\sigma}(s)\overline{Z}(s)} \frac{d\overline{\vartheta}(x,s)}{dx} \tag{19}$$

with inhomogeneous boundary conditions:

$$\bar{q}(x=0,s) = S_0 \overline{F}(s) \tag{20}$$

$$\bar{q}(x=l,s) = 0 \tag{21}$$

where $\overline{F}(s)$ is the Laplace transform of the time-dependent function that describes the evolution of optical excitation, Equations (8) and (9). Symbols $\overline{\vartheta}(x,s)$ and $\bar{q}(x,s)$ signify complex representative of equilibrium temperature variations and heat flux, respectively, and superscript bar in other symbols signify complex function of the complex variable s.

Parameters $\overline{\sigma}$ (complex coefficient of heat transfer) and $\overline{Z}$ (complex thermal impedance) are defined as follows:

$$\overline{\sigma} = \sqrt{\frac{s^v}{D_v}} \tag{22}$$

$$\overline{Z} = \frac{\sqrt{D_v}}{k}\sqrt{\frac{1}{s^v}} \tag{23}$$

By solving the above system of equations, Equations (18) and (19), with the boundary conditions, Equations (20) and (21), the spectral function of the profile of temperature variations in the sample is obtained, as well as surface temperature variations on the non-illuminated surface of the sample (sample/air boundaries):

$$\overline{\vartheta}(x,s) = S_0 \overline{Z}\frac{ch(\overline{\sigma}(l-x))}{sh(\overline{\sigma}l)}\overline{F}(s) \tag{24}$$

$$\overline{\vartheta}(l,s) = S_0 \overline{Z}\frac{1}{sh(\overline{\sigma}l)}\overline{F}(s) \tag{25}$$

If the local non-equilibrium is not taken into account and heat transfer is described by Equations (1)–(3), the classical model of the spectral function of the PA signal is obtained, where only the thermal impedances and the complex propagation coefficient differ than parameters given by Equations (22) and (23). In the classic model, these complex parameters are defined by the following expressions [66]:

$$\overline{\sigma}_{class} = \sqrt{\frac{s}{D}} \tag{26}$$

$$\overline{Z}_{class} = \frac{\sqrt{D}}{k}\sqrt{\frac{1}{s}} \tag{27}$$

Based on the RG theory [1], pressure fluctuations in the gaseous environment of an optically heated sample are depended on temperature variations at the sample/air boundary, if the length of the gas column is much larger than the thermal diffusion length in the gas,

$$\overline{p}(s) = \frac{p_0}{T_0}\frac{\sqrt{D_g}}{l_g}\frac{1}{\sqrt{s}}\overline{\vartheta}(l,s) \tag{28}$$

In Equation (28), the following symbols are introduced: p_0 and T_0 are normal pressure and temperature of ambient, D_g is thermal diffusivity in air, and l_g is air column length in PA cell, Figure 1.

Substituting Equation (25) into Equation (28), the spectral function of pressure fluctuations in the gaseous environment of the sample is obtained:

$$\overline{p}(s) = S_0 \frac{p_0}{T_0}\frac{\sqrt{D_g}}{l_g}\frac{1}{\sqrt{s}}\overline{Z}\frac{1}{sh(\overline{\sigma}l)}\overline{F}(s) \tag{29}$$

The model given by Equation (29) can be obtained from the Generalized Cattaneo Fractional Model GCEIII for thermal piston component of PA signal presented in paper [67] if inertial relaxations are neglected and if one finds the limit for the optically opaque sample.

Taking into account that the microphone, which records pressure fluctuations, behaves as a differentiator of these fluctuations [68], the spectral function of the recorded PA signal is described by the following expression:

$$\overline{S}(s) = AS_0 \frac{p_0}{T_0} \frac{\sqrt{D_g}}{l_g} \frac{s}{\sqrt{s}} \overline{Z} \frac{1}{sh(\overline{\sigma}l)} \overline{F}(s) \tag{30}$$

where A signifies the gain of electrical signal recorded by microphone.

To calculate time dependent PA signal for thin samples, we used the development function $sh(\overline{\sigma}l)/\overline{\sigma}l$ in power order as follows [69]:

$$\frac{sh(y)}{y} = 1 + \frac{y^2}{3!} + \frac{y^4}{5!} + \dots \tag{31}$$

By substituting Equations (22), (23) and (31) in Equation (30), an approximate spectral function of the PA signal is obtained, which includes the local non-equilibrium in complex systems:

$$\overline{S}(s) = Ka\sqrt{a} \frac{1}{s^{v-0.5}} \frac{1}{s^v + a} \overline{F}(s) \tag{32}$$

where

$$K = AS_0 \frac{p_0}{T_0} \frac{\sqrt{D_g}}{kl_g} \tag{33}$$

$$a = \frac{6D_v}{l^2} \tag{34}$$

In order to compare our model with the classical model, we first calculated the spectral function of the PA signal based on the classical theory of heat conduction. Substituting Equations (26), (27) and (31) in Equation (30) gives the following:

$$\overline{S}_{class}(s) = K_1 a_1 \sqrt{a_1} \frac{1}{\sqrt{s}} \frac{1}{s + a_1} \overline{F}(s) \tag{35}$$

where

$$K_1 = K = AS_0 \frac{p_0}{T_0} \frac{\sqrt{D_g}}{kl_g} \tag{36}$$

$$a_1 = \frac{6D}{l^2} \tag{37}$$

In further analysis, time-domain PA signals normalized to the gain constant K will be considered:

$$\overline{S}_n(s) = \frac{a\sqrt{a}}{s^{v-0.5}} \frac{1}{s^v + a} \overline{F}(s) \tag{38}$$

$$\overline{S}_{nclass}(s) = \frac{a_1 \sqrt{a_1}}{\sqrt{s}} \frac{1}{s + a_1} \overline{F}(s) \tag{39}$$

Considering that Laplace transforms of optical pulse given by Equation (8) is $\overline{F}(s) = 1$ [70], we obtain spectral functions of PA signals for very short optical pulse predicted by fractional and classical theory:

$$\overline{S}_n(s) = \frac{a\sqrt{a}}{s^{v-0.5}} \frac{1}{s^v + a} \tag{40}$$

$$\overline{S}_{nclass}(s) = \frac{a_1 \sqrt{a_1}}{\sqrt{s}} \frac{1}{s + a_1} \tag{41}$$

Similarly, for very long optical pulse described by Equation (9), we have $\overline{F}(s) = 1/s$ [68], and consequently, spectral functions of PA signals from Equations (38) and (39) become the following:

$$\overline{S}_n(s) = \frac{a\sqrt{a}}{s^{v+0.5}} \frac{1}{s^v + a} \tag{42}$$

$$\overline{S}_{nclass}(s) = \frac{a_1\sqrt{a_1}}{s\sqrt{s}} \frac{1}{s + a_1} \tag{43}$$

Normalized PA signals in the time domain were obtained by finding the inverse Laplace transform of Equations (40)–(43).

As it can be seen from Equations (41) and (43), the spectral functions predicted by the classical model are described by the product of fractional operator and rational function $1/(s + a_1)$ which inverse Laplace transforms given in Table 1, are known [70].

Table 1. Table of inverse Laplace transform of some rational and irrational functions [70].

Laplace Transform $G(s)$	Inverse Laplace Transform $L^{-1}[G(s)]$
$\dfrac{1}{\sqrt{s}}$	$\dfrac{1}{\sqrt{\pi t}}$
$\dfrac{1}{s\sqrt{s}}$	$2\sqrt{\dfrac{t}{\pi}}$
$\dfrac{1}{s + a}$	e^{-at}

As it is known, product in s-space is convolution in time. Inverse Laplace transform of spectral function given by Equation (41) is obtained by solution of convolution integral:

$$S_{nclass}(t) = a_1\sqrt{a_1}\int_0^t \frac{1}{\sqrt{\pi t'}}e^{-a_1(t-t')}dt' = a_1\sqrt{a_1}e^{-t^2}\int_0^t e^{(at')^2}dt' \tag{44}$$

Using the results of the paper [71], the above solution can be represented via the two-parameter Mittag-Leffler function [50,72]:

$$S_{nclass}(t) = a_1\sqrt{a_1}t^{v-0.5}E_{v,v+0.5}(-a_1t^v) \tag{45}$$

where Mittage-Leffler function is defined by the following [72]:

$$E_{\alpha,\beta}^{\gamma}(z) = \sum_{k=1}^{\infty} \frac{(\gamma)_k}{\Gamma(\alpha k + \beta)} \frac{z^k}{k!} \tag{46}$$

with Pochhammer symbol defined by the following:

$$(\gamma)_k = \gamma(\gamma + 1)(\gamma + 2)\ldots(\gamma + k - 1) \tag{47}$$

The inverse Laplace transform of the function given by Equation (43), for PA signal of long optical pulse, is found by solving the following convolution integral:

$$S_{nclass}(t) = a_1\sqrt{a_1}\int_0^t h(t - t')t'^{v-0.5}E_{v,v+0.5}\left(-a_1t'^v\right)dt' \tag{48}$$

Using the properties of the Mittag-Leffler function [50,71–73], the solution of the above integral is again a two-parameter Mittag-Leffler function:

$$S_{nclass}(t) = a_1\sqrt{a_1}t^{v+0.5}E_{v,v+1.5}(-a_1t^v) \tag{49}$$

The spectral functions of the PA signal for the fractional model are given by Equations (40) and (42), for very short optical pulse and for long optical pulse, respectively. As can be seen from these expressions, both functions are given as a product of functions described by irrational operators. To find their inverse Laplace transform, the general solution [74] given in Table 2 was used.

Table 2. Inverse Laplace transform of some irrational order functions [74].

Laplace Transform $F(s)$	Inverse Laplace Transform $L^{-1}[F(s)]$
$\dfrac{s^{\alpha\gamma-\beta}}{(s^{\alpha}+a)^{\gamma}}$	$t^{\beta-1}E_{\alpha,\beta}^{\gamma}(-at^{\alpha})$

By using Equation (40) and Table 2, the time-domain PA signal for very short optical pulse is given by the following:

$$S_n(t) = a\sqrt{a}t^{2v-1.5}E_{v,2v-0.5}(-at^v) \tag{50}$$

In a similar way, the time domain PA signal generated by long optical pulse for which spectral function is given by Equation (42) is obtained:

$$S_n(t) = a\sqrt{a}t^{2v-0.5}E_{v,2v+0.5}(-at^v) \tag{51}$$

4. Discussion

By comparing the expressions describing the PA signal predicted by the fractional model Equations (50) and (51) with the expressions describing the PA signal predicted by the classical model Equations (45) and (49), for both types of optical impulse excitation, it is shown that the fractional models reduce to the classical for $v = 1$.

In order to examine the influence of the local non-equilibrium represented by the fractional exponent v on the time-domain PA signal generated by a very short optical excitation, we illustrated the PA signals described by Equations (48) and (50) in Figure 2 for $a = a_1 = 1$ and several values of the fractional exponent v from the range (0,1).
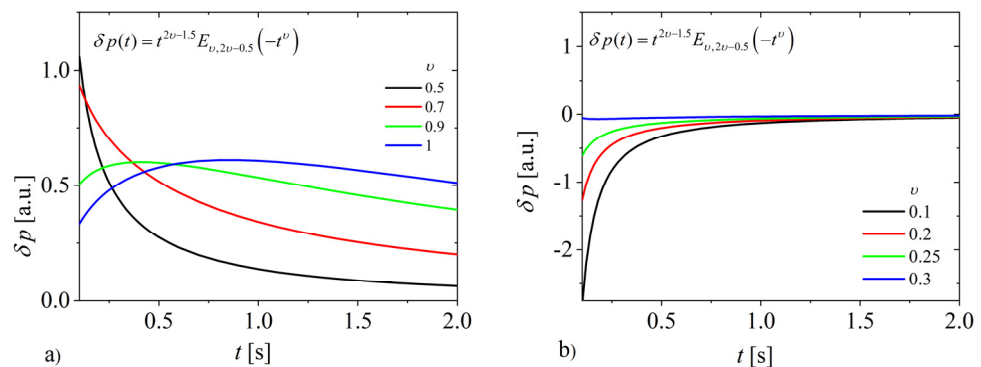
Figure 2. Photoacoustic signal induced by very short optical pulse (Equations (48) and (50)) for (**a**) $v > 0.3$ (**b**) $v < 0.3$.

It can be seen from Figure 2a that for $t < 0.5$ s and $0.3 < v < 0.8$ the fractional model predicts a completely different behavior of the PA signal (steep decline) than the classic diffusion model ($v = 1$, blue line in Figure 2), while in the long time domain, both models, fractional for $v > 0.3$ and classical, predict decreasing signal. The completely different pattern in short time domain predicted by fractional model for $0.3 < v < 0.8$ can be explained by the fact that Equation (5) with the Riemann–Liouville definition of the fractional derivative (Equation (6)), is not equivalent to the integral representation of the First Law of Thermodynamics Equation (4) for any initial conditions as discussed in [75]. Riemann–Liouville fractional derivatives are non-local operators that are non-invariant

under time reversal and can be recognized as infinitesimal generators of a coarse-grained microscopic time evolution which is not sufficient for description evolution in a short time limit [75–77]. This means that the derived model can be applied to the consideration of PA signals excited by very short pulse in the long time domain if $v > 0.3$. In this domain, the fractional model predicts smaller signal values and their rapid decline towards a steady value. The classical model predicts a decreasing function proportional to $1/\sqrt{t}$, while fractional models predict a decreasing function proportional to $1/t^{1.5-v}$ in the long-time domain. Physically, it means the following: if the fractional exponent v decreases, the kinetic relaxations become slower leading to an increase in the diffusion length of heat and more rapid convergence to a steady state after very short pulse excitation.

For $v < 0.3$, the derived model predicts completely non-physical behavior of the PA signal, see Figure 2b. It seems that the system can be optically cooled generating sub-pressure in the air environment if there are structural elements that slowly relax. However, we think that the flow of heat in a medium in which there are very slow relaxations, i.e., large degrees of freedom of the structural elements, cannot be well physically described either short-time domain or longtime domain without taking into account non-zero initial conditions (see consideration of Fourier's and Maxwell's materials [27,28]). From the point of view of material physics, it means that for $v < 0.3$, there is phase transition of solids in some more fluid phases indicating a different description of heat transfer. It means that the domain of validity of the derived model is limited to systems with fractional exponents $v > 0.3$.

From Figure 3, it can be seen that the PA signal excited by a very long optical pulse in the long time-domain grows more slowly than predicted by the classical model ($v = 1$, magenta line). As v decreases, the time constant of the PA signal increases. The slower the kinetic relaxation, the smaller the fractional exponent and the diffusion length of heat carriers decrease. It is the cause of the smaller slope of the PA signal and its higher time constant.
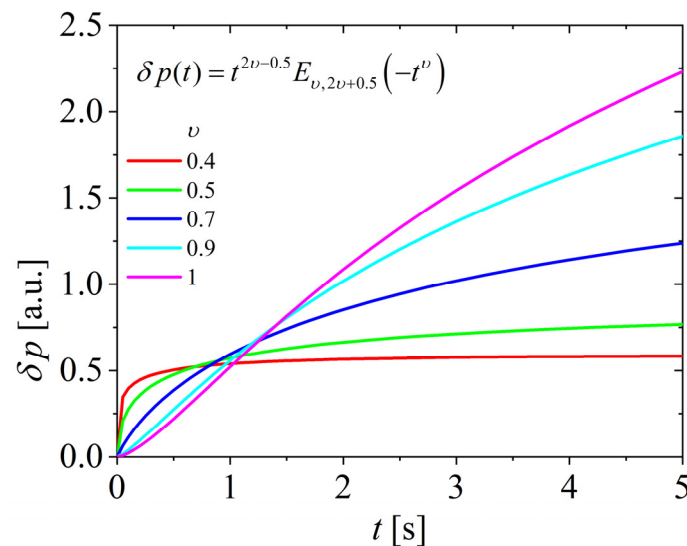
Figure 3. The PA signals excited by very long optical pulse (described by Equations (49) and (51)) for $a = 1$ and several values of the fractional exponent v from the range $(0, 1)$.

It is important to note that the fractional as well as the classical model predict PA signal divergence in the long time domain, Figure 3. We think that the cause of this behavior is related to the limitations of the thermal piston model [17,62,68]. Namely, this model, as discussed in [62,68], presupposes that the diffusion length of heat in the gas is much smaller than the dimensions of the cells. This assumption is completely justified for harmonics whose frequency is higher than 100 Hz [1], but for lower harmonics of very long pulse excitation, whose influence becomes expressed in the long time domain, this assumption is

not justified, and for a complete analysis of the PA signal, it is necessary to use a generalized model of transformation of variation temperatures at the sample/gas boundary in pressure fluctuations in a PA cell of finite length [68].

The influence of sample thickness on PA signals excited by very short optical pulse and very long optical pulse are illustrated in Figure 4.
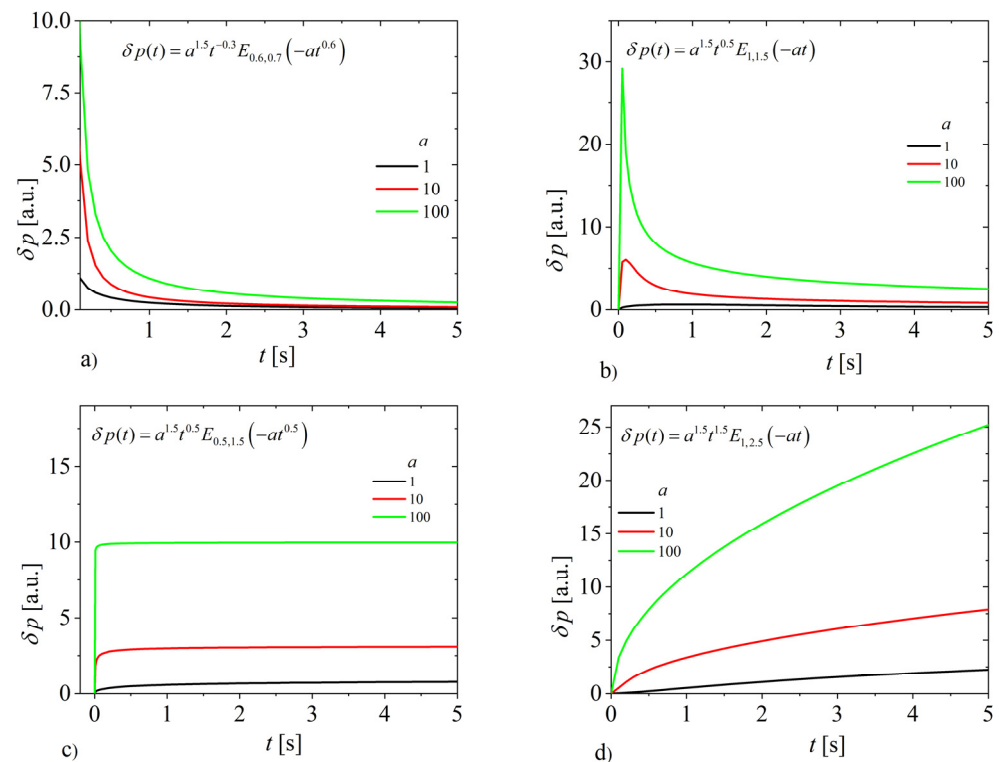
Figure 4. The dependence of PA signal on sample thickness (**a**) $v = 0.6$, short pulse excitation; (**b**) $v = 1$, short pulse excitation, (**c**) $v = 0.5$, long pulse excitation; and (**d**) $v = 1$, long pulse excitation.

As it could be seen from Figure 4a,b, for a very short excitation pulse, decreasing the thickness of the sample affects the shift of the boundary between the short and long time domains to the right, opposite to the effect of decreasing the fractional exponent (as it is discussed below in Figure 2, the different pattern obtained by the fractional model and short pulse excitation in the short time domain in relation to the classical model is a consequence of zero initial conditions and the Riemann–Liouville definition of the fractional derivative). However, for a long excitation pulse, the reduction of the sample thickness affects the shift of the boundary between the short and long time domains towards a shorter time interval compared to the initial moment, Figure 4c. A similar effect can be observed in Figure 3 if the fractional exponent decreases.

For both types of excitations, the thinner the sample, the higher the PA signal in each moment. Additionally, the signal pattern is similar for each thickness and follows the excitation shape if $v < 1$. Physically, it can be explained by the decrease in the mean square displacement of heat carriers if there are kinetic relaxations i.e., local non-equilibrium.

5. Conclusions

In the paper, a generalized theoretical description of optically excited surface temperature variations in samples with a complex internal structure is performed, taking into account the local non-equilibrium of subsystems with large kinetic degrees of freedom that are expected to exist in such complex samples. In that case, the local non-equilibrium is taken into account through the fractional exponent and fractional thermal diffusivity.

It is shown that the obtained theoretical description can coincide with the one obtained in the framework of statistical physics, which is based on the consideration of anomalous

diffusion effects, i.e., the deviation of the mean square displacement of heat carriers from the linear law. Using a generalized description of heat conduction, a fractional model of the spectral function of surface temperature variations and pressure fluctuations in the gaseous environment of the optically excited sample was derived. Derived expressions are validated by comparison with spectral functions obtained by the classical model and previous fractional models.

Based on the fractional model of the spectral function of pressure fluctuations, a time-domain PA signal was derived for very short and very long pulse excitations. Comparing it with the classical model, it was shown that the derived model reduces to the classical one when the fractional exponent is equal to unity.

Analysis of the PA signal for the very short optical excitation showed that the domain of validity of the derived fractional model is limited to a long time domain. For such excitations, fractional models predict a smaller time constant of the signal than the classic one due to the influence of local non-equilibrium on the decrease in the thermal diffusion length of the sample with a complex internal structure.

The analysis of the PA signal for very long optical excitation pointed out the shortcomings of the classic thermal piston model, which is widely used in frequency photoacoustics. For long pulsed excitations, low harmonics of time-dependent temperature variations at the sample/air interface, whose diffusion length is greater than the cell dimensions, must be taken into account. However, in the long time limit, it can be clearly observed that the local non-equilibrium affects the higher time constant of the PA signal, which is related to the subdiffusion nature of heat propagation through the sample in which there are slow kinetic relaxations.

The sample thickness influences the magnitude of the PA signal. The signal is larger for a thinner sample.

Our results show that time-domain photoacoustics could be applied to the estimation of the rate of non-equilibrium relaxations in complex systems, but it requires further development of the model of the PA signal in the time domain as well as a fractional model of heat conduction.

Author Contributions: Conceptualization, S.G.; methodology, S.G.; software, A.I.D.; validation, S.G., A.I.D., B.Z.K., K.L.D. and D.C.; formal analysis, S.G., A.I.D., B.Z.K., K.L.D. and D.C.; investigation, S.G., A.I.D., B.Z.K., K.L.D. and D.C.; resources, S.G., A.I.D., B.Z.K., K.L.D. and D.C.; data curation, D.C; writing—original draft preparation, S.G.; writing—review and editing, S.G., K.L.D. and D.C.; visualization, A.DJ. and K.L.D.; supervision, S.G. and K.L.D.; project administration, D.C.; funding acquisition, D.C All authors have read and agreed to the published version of the manuscript.

Data Availability Statement: The authors confirm that the data supporting the findings of this study are available within the article.

Conflicts of Interest: The authors declare no conflicts of interest.

References

1. Rosencwaig, A.; Gersho, A. Theory of the photoacoustic effect with solids. *J. Appl. Phys.* **1976**, *47*, 64–69. [CrossRef]
2. Tam, A.C. Applications of photoacoustic sensing techniques. *Rev. Mod. Phys.* **1986**, *58*, 381–431. [CrossRef]
3. Park, H.K.; Grigoropoulos, C.P.; Tam, A.C. Optical measurements of thermal diffusivity of a material. *Int. J. Thermophys.* **1995**, *16*, 973–995. [CrossRef]
4. Vargas, H.; Miranda, L.C.M. Photoacoustic and related photothermal techniques. *Phys. Rep.* **1988**, *161*, 43–101. [CrossRef]
5. Bialkowski, S. *Photothermal Spectroscopy Methods for Chemical Analysis*; John Wiley: New York, NY, USA, 1996; ISBN 978-1-119-27907-5.
6. Sarode, A.P.; Mahajan, O.H. Theoretical Aspects of Photoacoustic Effect with Solids: A Review. *Int. J. Sci. Adv. Res. Technol.* **2018**, *4*, 1237–1242. [CrossRef]

7. Isaiev, M.; Mussabek, G.; Lishchuk, P.; Dubyk, K.; Zhylkybayeva, N.; Yar-Mukhamedova, G.; Lacroix, D.; Lysenko, V. Application of the Photoacoustic Approach in the Characterization of Nanostructured Materials. *Nanomaterials* **2022**, *12*, 708. [CrossRef] [PubMed]

8. Mandelis, A.; Royce, B.S.H. Time-domain photoacoustic spectroscopy of solids. *J. Appl. Phys.* **1979**, *50*, 4330–4338. [CrossRef]

9. Mandelis, A.; Hess, P. *Semiconductors and Electronic Materials*; SPIE Opt. Eng. Press: Belingham, WA, USA, 2000; ISBN 0819435066.

10. Olenka, L.; Nogueiran, E.S.; Medina, A.N.; Baesso, M.L.; Bento, A.C.; Muniz, E.C.; Rubira, A.F. Photoacoustic study of PET films and fibers dyed in supercritical CO2 reactor. *Rev. Sci. Instrum.* **2003**, *74*, 328–330. [CrossRef]

11. Pichardo-Molina, J.L.; Gutiérrez-Juárez, G.; Huerta-Franco, R.; Vargas-Luna, M.; Cholico, P.; Alvarado-Gil, J.J. Open Photoacoustic Cell Technique as a Tool for Thermal and Thermo-Mechanical Characterization of Teeth and Their Restorative Materials. *Int. J. Thermophys.* **2005**, *26*, 243–253. [CrossRef]

12. Lishchuk, P.; Isaiev, M.; Osminkina, L.; Burbelo, R.; Nychyporuk, T.; Timoshenko, V. Photoacoustic characterization of nanowire arrays formed by metal-assisted chemical etching of crystalline silicon substrates with different doping level. *Phys. E Low-Dimens. Syst. Nanostructures* **2019**, *107*, 131–136. [CrossRef]

13. Lishchuk, P.; Andrusenko, D.; Isaiev, M.; Lysenko, V.; Burbelo, R. Investigation of Thermal Transport Properties of Porous Silicon by Photoacoustic Technique. *Int. J. Thermophys.* **2015**, *36*, 2428–2433. [CrossRef]

14. Dubyk, K.; Borisova, T.; Paliienko, K.; Krisanova, N.; Isaiev, M.; Alekseev, S.; Skryshevsky, V.; Lysenko, V.; Geloen, A. Bio-distribution of Carbon Nanoparticles Studied by Photoacoustic Measurements. *Nanoscale Res. Lett.* **2022**, *17*, 127. [CrossRef]

15. Li, C.; Wang, L.V. Photoacoustic tomography and sensing in biomedicine. *Phys. Med. Biol.* **2009**, *54*, 59–97. [CrossRef]

16. Somer, A.; Camilotti, F.; Costa, G.F.; Bonardi, C.; Novatski, A.; Andrade, A.V.C.; Kozlowski, V.A.; Cruz, G.K. The thermoelastic bending and thermal diffusion processes influence on photoacoustic signal generation using open photoacoustic cell technique. *J. Appl. Phys.* **2013**, *114*, 063503. [CrossRef]

17. Bein, B.; Pelzl, J. Theory of signal generation in a photoacoustic cell. *J. Phys. Colloq.* **1983**, *44*, 6–27. Available online: https://hal.science/jpa-00223163 (accessed on 27 June 2024). [CrossRef]

18. Carslaw, H.S.; Jaeger, J.C. *Conduction of Heat in Solids*; Oxford University Press: Oxford, UK, 1959; ISBN 0198533683.

19. Sobolev, S.L. Local non-equilibrium transport models. *Phys. Uspekhi* **1997**, *167*, 1095–1106. [CrossRef]

20. Sobolev, S.L.; Dai, W. Heat Transport on Ultrashort Time and Space Scales in Nanosized Systems: Diffusive or Wave-like? *Materials* **2022**, *15*, 4287. [CrossRef] [PubMed]

21. Sobolev, S.L. Hyperbolic heat conduction, effective temperature, and third law for nonequilibrium systems with heat flux. *Phys. Rev. E* **2018**, *97*, 022122. [CrossRef]

22. Sobolev, S.L. Effective temperature in nonequilibrium state with heat flux using discrete variable model. *Phys. Lett. A* **2017**, *381*, 2893–2897. [CrossRef]

23. Garden, J.L. Macroscopic non-equilibrium thermodynamics in dynamic calorimetry. *Thermochim. Acta* **2007**, *452*, 85–105. [CrossRef]

24. Garden, J.L.; Richard, J.; Saruyama, Y. Entropy production in TMDSC. *J. Therm. Anal. Calorim.* **2008**, *94*, 585–590. Available online: https://hal.science/hal-00311748 (accessed on 27 June 2024). [CrossRef]

25. Birge, N.O. Specific-heat spectroscopy of glycerol and propylene glycol near the glass transition. *Phys. Rev. B* **1986**, *34*, 1631–1642. [CrossRef] [PubMed]

26. Birge, N.O.; Nagel, S.R. Specific-heat spectroscopy of the glass transition. *Phys. Rev. Lett.* **1985**, *54*, 2674–2677. [CrossRef]

27. Novikov, I.A.; Kolpashchikov, V.L.; Shnip, A.I. *Rheophysics and Heat Physics of Nonequilibrium Systems*; Izd. Akad. Nauk Belorus. SSR: Minsk, Belarus, 1991. (In Russian)

28. Novikov, I.A. Harmonic thermal waves in materials with thermal memory. *J. Appl. Phys.* **1997**, *81*, 1067–1072. [CrossRef]

29. Tzou, D.Y. *Macro-to-Microscale Heat Transfer: The Lagging Behavior*; Taylor and Francis: Washington, DC, USA, 1996; pp. 323–332. Available online: https://lib.ugent.be/catalog/rug01:001873084 (accessed on 27 June 2024).

30. Wunderlih, B. *Thermal Analysis of Polymeric Materials*; Springer: Berlin/Heidelberg, Germany; New York, NY, USA, 2005.

31. Roetzel, W.; Putra, N.; Das, S.K. Experiment and analysis for non-Fourier conduction in materials with non-homogeneous inner structure. *Int. J. Therm. Sci.* **2003**, *42*, 541–552. [CrossRef]

32. Dixon, P.K. Specific-heat spectroscopy and dielectric susceptibility measurements of salol at the glass transition. *Phys. Rev. B* **1990**, *42*, 8179–8186. [CrossRef] [PubMed]

33. Scherrenberg, R.; Mathot, V.; Steeman, P. The Applicability of TMDSC to Polymeric Systems General theoretical description based on the full heat capacity formulation. *J. Therm. Anal. Calorim.* **1998**, *54*, 477–499. [CrossRef]

34. Saiter, A.; Couderc, H.; Grenet, J. Characterisation of structural relaxation phenomena in polymeric materials from thermal analysis investigations. *J. Therm. Anal. Calorim.* **2007**, *88*, 483–488. [CrossRef]

35. Saruyama, Y. AC calorimetry at the first order phase transition point. *J. Therm. Anal.* **1992**, *38*, 1827–1833. [CrossRef]

36. Liu, K.C.; Wang, Y.; Chen, Y. Investigation of the bioheat transfer with dual phase lag effect. *Int. J. Therm. Sci.* **2012**, *58*, 29–35. [CrossRef]

37. Mitra, K.; Kumar, S.; Vedavarez, A.; Moallemi, M.K. Experimental Evidence of Hyperbolic Heat Conduction in Processed Meat. *J. Heat Transf.* **1995**, *117*, 568–573. [CrossRef]

38. Djordjevic, K.L.; Milicevic, D.; Galovic, S.P.; Suljovrujic, E.; Jacimovski, S.K.; Furundzic, D.; Popovic, M. Photothermal Response of Polymeric Materials Including Complex Heat Capacity. *Int. J. Thermophys.* **2022**, *43*, 68. [CrossRef]

39. Jou, D.; Casas-Vazquez, J.; Lebon, G. Extended irreversible thermodynamics. *Rep. Prog. Phys.* **1988**, *51*, 1105–1179. [CrossRef]

40. Davies, R.O. The Macroscopic Theory of Irreversibility. *Rep. Prog. Phys.* **1956**, *19*, 326–367. [CrossRef]

41. De Groot, S.R.; Mazur, P. *Non-Equilibrium Thermodynamics*; North-Holland Publishing Company: Amsterdam, The Netherands, 1962; ISBN 0486153509.

42. Prigogine, I. *Introduction to Thermodynamics of Irreversible Processes*; John Wiley and Sons: New York, NY, USA, 1968; ISBN 0470699280.

43. Metzler, R.; Klafter, J. The random walk's guide to anomalous diffusion: A fractional dynamics approach. *Phys. Rep.* **2000**, *339*, 1–77. [CrossRef]

44. Korabel, N.; Klages, R.; Chechkin, A.V.; Sokolov, I.M.; Gonchar, V.Y. Fractal properties of anomalous diffusion in intermittent maps. *Phys. Rev. E* **2007**, *75*, 036213. [CrossRef] [PubMed]

45. Bouchaud, J.-P.; Georges, A. Anomalous diffusion in disordered media: Statistical mechanisms, models and physical applications. *Phys. Rep.* **1990**, *195*, 127–293. [CrossRef]

46. Liang, Y.; Wang, W.; Metzler, R. Anomalous diffusion, non-Gaussianity, and nonergodicity for subordinated fractional Brownian motion with a drift. *arXiv* **2023**, arXiv:2302.04872v1. [CrossRef] [PubMed]

47. Metzler, R.; Rajyaguru, A.; Berkowitz, B. Modelling anomalous diffusion in semi-infinite disordered systems and porous media. *New J. Phys.* **2022**, *24*, 123004. [CrossRef]

48. Sposini, V.; Krapf, D.; Marinari, E.; Sunyer, R.; Ritort, F.; Taheri, F.; Selhuber-Unkel, C.; Benelli, R.; Weiss, M.; Metzler, R.; et al. Towards a robust criterion of anomalous diffusion. *Commun. Phys.* **2022**, *5*, 305. [CrossRef]

49. Comptey, A.; Metzler, R. The generalized Cattaneo equation for the description of anomalous transport processes. *J. Phys. A Math. Gen.* **1997**, *30*, 7277–7289. [CrossRef]

50. Gorenflo, R.; Kilbas, A.A.; Mainardi, F.; Rogosin, S.V. *Mittag-Leffler Functions, Related Topics and Applications*; Springer: Berlin/Heidelberg, Germany, 2014; ISBN 978-3-662-43930-2. (eBook). [CrossRef]

51. Kiryakova, V.S. *Generalized Fractional Calculus and Applications*; Longman Scientific and Technical: Harlow, UK, 1994.

52. Podlubny, I. *Fractional Differential Equations*; Academic Press: San Diego, CA, USA, 1999.

53. Tateishi, A.A.; Lenzi, E.K.; Da Silva, L.R.; Ribeiro, H.V.; Picoli, S.; Mendes, R.S. Different diffusive regimes, generalized Langevin and diffusion equations. *Phys. Rev. E* **2012**, *85*, 011147. [CrossRef] [PubMed]

54. Dzielinski, A.; Sierociuk, D.; Sarwas, G. Some applications of fractional order calculus. *Bull. Pol. Acad. Sci. Tech. Sci.* **2010**, *58*, 583–592. [CrossRef]

55. Lenzi, E.K.; Somer, A.; Zola, R.S.; Da Silva, R.S.; Lenzi, M.K.A. Generalized Diffusion Equation: Solutions and Anomalous Diffusion. *Fluids* **2003**, *8*, 34. [CrossRef]

56. Caputo, M.; Fabrizio, M. Admissible frequency domain response functions of dielectrics. *Math. Method Appl. Sci.* **2014**, *38*, 930–936. [CrossRef]

57. Saxena, R.K.; Saxena, R.; Kalla, S.L. Solution of space time fractional schroedinger equation occurring in quantum mechanics. *Fract. Calc. Appl.* **2010**, *13*, 190–201. Available online: http://hdl.handle.net/10525/1648 (accessed on 27 June 2024).

58. Del Castillo Negrete, D.; Carreras, B.A.; Lynch, V.E. Fractional diffusion in plasma turbulence. *Phys. Plasmas* **2004**, *11*, 3854–3864. [CrossRef]

59. Magin, R.L. *Fractional Calculus in Bioengineering*; Begell House Publishers: New York, NY, USA, 2006.

60. Djordjević, K.L.; Stoisavljević, Z.Z.; Dragaš, M.A.; Stanimirović, I.; Stanimirović, Z.; Suljovrujic, E.; Galović, S.P. Application of neural network to study of frequency range effect to photoacoustic measurement of thermoelastic properties of thin aluminum samples. *Measurement* **2024**, *236*, 115043. [CrossRef]

61. Miletic, V.V.; Popovic, M.N.; Galovic, S.P.; Markushev, D.D.; Nesic, M.V. Photothermally induced temperature variations in a low-absorption sample via backside absorption. *J. Appl. Phys.* **2023**, *133*, 075101. [CrossRef]

62. Galovic, S.P.; Stanimirovic, Z.; Stanimirovic, I.; Djordjevic, K.L.; Milicevic, D.; Suljovrujic, E. Time-resolved photoacoustic response of thin solids measured using minimal volume cell. *Int. Commun. Heat Mass Transf.* **2024**, *155*, 107574. [CrossRef]

63. Sablikov, V.A.; Sandomirskii, V.B. The Photoacoustic effect in semiconductors. *Phys. Stat. Solidi (a)* **1983**, *120*, 471–480. [CrossRef]

64. Galović, S.; Šoškić, Z.; Popović, M.; Čevizović, D.; Stojanović, Z. Theory of photoacoustic effect in media with thermal memory. *J. Appl. Phys.* **2014**, *116*, 024901. [CrossRef]

65. Polyanin, A.D.; Sorokin, V.G.; Zhurov, A.I. *Delay Ordinary and Partial Differential Equation*; CRC Press: Boca Raton, FL, USA, 2024. [CrossRef]

66. Galović, S.; Kostoski, D. Photothermal wave propagation in media with thermal memory. *J. Appl. Phys.* **2003**, *93*, 3063–3070. [CrossRef]

67. Somer, A.; Galovic, S.; Lenzi, E.K.; Novatski, A.; Djordjevic, K. Temperature profile and thermal piston component of photoacoustic response calculated by the fractional dual-phase-lag heat conduction theory. *Int. J. Heat Mass Transf.* **2023**, *203*, 123801. [CrossRef]

68. Galovic, S.P.; Djordjevic, K.L.; Nesic, M.V.; Popovic, M.N.; Markushev, D.D.; Markushev, D.K.; Todorovic, D.M. Time-domain minimum-volume cell photoacoustic of thin semiconductor layer. *I. Theory. J. Appl. Phys.* **2023**, *133*, 245701. [CrossRef]

69. Galovic, S.; Soskic, Z.; Popovic, M. Analysis of photothermal response of thin solid films by analogy with passive linear electric networks. *Therm. Sci.* **2009**, *13*, 129–142. [CrossRef]

70. Roberts, G.E.; Kaufman, H. *Table of Laplace Transform*; W.B. Saunders Company: Philadelphia, PA, USA; London, UK, 1966.

71. Saenko, V.V. Integral Representation of the Mittag-Leffler Function. *Russ. Math.* **2022**, *66*, 43–58. [CrossRef]

72. Haubold, H.J.; Mathai, A.M.; Saxena, R.K. Mittag-Leffler Functions and Their Applications. *J. Appl. Math.* **2011**, *2011*, 298628. [CrossRef]

73. Baumann, G. Sinc Based Inverse Laplace Transforms, Mittag-Leffler Functions and Their Approximation for Fractional Calculus. *Fractal Fract.* **2021**, *5*, 43. [CrossRef]

74. Chen, Y.Q.; Petras, I.; Vinagre, B.M. A list of Laplace and Inverse Laplace Transforms Related to Fractional Order Calculus. 2007. Available online: http://www.tuke.sk/petras/foc_laplace.pdf (accessed on 27 June 2024).

75.   Hilfer, R. Fractional Diffusion Based on Riemann-Liouville Fractional Derivatives. *J. Phys. Chem. B* **2000**, *104*, 3914–3917. [CrossRef]
76.   Abdon, A.; Gómez-Aguilar, J.F. Decolonisation of fractional calculus rules: Breaking commutativity and associativity to capture more natural phenomena. *Eur. Phys. J. Plus* **2018**, *133*, 166. [CrossRef]
77.   Tateishi, A.A.; Ribeiro, H.V.; Lenzi, E.K. The role of the fractional time-derivative operators in anomalous diffusion. *Front. Phys.* **2017**, *5*, 52. [CrossRef]